Detection of the freezing state and frozen section thickness of fine sand by ultrasonic testing

Article (Published Version)

Received: 29 October 2019 | Revised: 19 March 2020 | Accepted: 11 May 2020

DOI: 10.1002/ppp.2075

WILEY

RESEARCH ARTICLE

Detection of the freezing state and frozen section thickness of fine sand by ultrasonic testing

Ji-wei Zhang[1,2,3,4] | Julian Murton[4] | Shu-jie Liu[1,2,3,5] | Li-li Sui[6] | Song Zhang[1,2,3,7]

[1]Shaft Construction Branch, China Coal Research Institute, Beijing, China

[2]Tian Di Science & Technology Co. Ltd, Beijing, China

[3]Beijing China Coal Mine Engineering Co. Ltd, Beijing, China

[4]Permafrost Laboratory, Department of Geography, University of Sussex, Brighton, UK

[5]University of Science and Technology Beijing, Beijing, China

[6]North China Institute of Science and Technology, Beijing, China

[7]School of Civil Engineering, Shijiazhuang Tiedao University, Hebei, China

Correspondence
Ji-wei Zhang and Shu-jie Liu, Shaft Construction Branch, China Coal Research Institute. Beijing 100013, China.
Email: zhangjiwei2018@sina.com; qiyijianjunyi@sina.com

Funding information
China Scholarship Council, Grant/Award Number: 201909110045; National Key Research and Development Plan of China, Grant/Award Number: 2016YFC0600904; National Natural Science Foundation of China, Grant/Award Numbers: 51804157, 5177040737, 11702094; North China Institute of Science and Technology Applied Mathematics Innovation Team, Grant/Award Number: 3142018059; Science and Technology Innovation Fund of TianDi science and technology co., LTD, Grant/Award Numbers: 2018-TD-QN008, 2018-TD-ZD004, 2019-TD-QN009

Abstract

Determining the freezing state and frozen section thickness is fundamental to assessing the development of artificial frozen walls but is commonly difficult or inaccurate because of a limited number and fixed position of thermometer holes under complex field conditions. We report a novel experimental design that measures soil temperature, water content, and ultrasonic properties to monitor movement of the cryofront (0°C isotherm), water migration, and acoustic parameters during progressive upward freezing of fine sand under laboratory conditions. Ultrasonic testing during different stages of freezing revealed changes in three acoustic parameters (wave velocity, wave amplitude, and frequency spectrum). As the cryofront ascended through the sand at different water contents, wave velocity continually increased, whereas wave amplitude initially decreased and then increased. Wave velocity measurements revealed the cryofront position during freezing, but measurements of wave amplitude did not. The frequency components indicated the frequency of different evolving freezing regions during upward freezing and the freezing state of fine sand during later stages of freezing. The freezing state can be evaluated on the basis of single vs multiple peaks and the kurtosis of frequency spectrum change. An equation developed to predict the thickness of the frozen section and tested against measured values in the laboratory and field showed accuracies of 86.84–99.33%. The equation is used successfully to estimate frozen wall thickness in artificially frozen fine sand in Guangzhou, China.

KEYWORDS

acoustic parameters, frozen sand, progressive upward freezing, ultrasonic testing

1 | INTRODUCTION

It is well known that artificial ground freezing is a preferred construction method of mine shafts and underground urban space in water-rich sand layers (e.g., [1–4]). The resulting artificial frozen walls, however, are commonly of inadequate thickness and strength because of substantial groundwater seepage, which can result in water inrush and abrupt subsidence (e.g., [5,6]). Thus,

determining the freezing state and frozen section thickness during freezing is fundamental to assessing the development of artificial frozen walls.

Several methods have been used to measure the freezing state and frozen section thickness with varying success. Real-time temperature monitoring[7] and theoretical derivation of stationary temperature fields[8] were used in the 1950s–1960s, whereas numerical simulations of nonstationary temperature fields have developed in recent decades (e.g., [9,10]). However, the freezing state and frozen section thicknesses predicted from these methods often differ from actual conditions at many sites with high groundwater seepage and geologic structures such as faults, cavities and interbedded strata, because the shape of frozen walls becomes irregular in these conditions. Ground-penetrating radar (GPR) has also been used to determine the freezing state and thickness of frozen walls,[11] although its results are affected by steel freezing pipes and a limited detection depth (3–30 m). Overall, therefore, a more accurate detection method is needed to determine the frozen wall thickness and freezing state. To this end, the present study investigates the use of ultrasonic testing.

Ultrasonic testing is an effective technique to identify the physical and mechanical parameters of frozen soil in the laboratory because soils that are fully or partially saturated with water experience large variations in acoustic parameters when they freeze (e.g., [12–15]). Several previous studies have investigated the relationships between acoustic parameters and physical mechanical properties of frozen soil (e.g., [16–22]). Wang et al.,[16] measured the wave velocity range of three frozen soils (Harbin clay, Lanzhou loess and Peking fine sand) at different temperatures: 2.124–2.727, 3.31–3.606 and 3.679–3.892 km/s, respectively. Christ and Park[17] investigated the correlation between acoustic properties of frozen soils and their physical–mechanical properties and used the ultrasonic method to evaluate the unfrozen water content and elasticity of frozen soils. Li et al.,[18] Li et al.,[19] and Huang et al.,[20] used wave velocity to evaluate the physical and mechanical properties of frozen silty clay. Their results indicate that changes in the physical mechanical properties of frozen soils can be measured indirectly by ultrasonic waves.[23] However, these studies focus on the change of acoustic parameters of frozen soil rather than soil that is freezing progressively. Therefore, there remain questions arising from the responses of acoustic parameters from progressively freezing soil, which is the basis of determining the freezing state and frozen section thickness of artificial freezing walls.

Here, we report a novel experimental design that measures soil temperature, water content, and ultrasonic properties to monitor movement of the cryofront (0°C isotherm), water migration, and acoustic parameters during progressive upward freezing of fine sand. This enables us to determine how acoustic parameters vary during progressive upward freezing and elucidate how ultrasonic testing can be used to estimate the freezing state and frozen section thickness. This work is part of a larger project examining the acoustic parameters and physical properties of frozen fine sand.[23]

Research Highlight

- Wave velocity, unlike wave amplitude, can reveal the cryofront position during partial freezing of fine sand.
- The frequency components during later stages of freezing can reveal the frequency of different freezing regions.
- Single and multiple peaks in the frequency spectrum and wave velocity during different stages of freezing can identify the freezing state.
- An equation is proposed to calculate the thickness of the frozen section, and it can be used to predict frozen wall thickness of fine sand in the laboratory and field.

2 | MATERIALS AND METHODS

2.1 | Soil properties and specimen preparation

Sand was obtained from 16 m depth at Baiyun Airport, Guangzhou, China. The physical properties of the sand, measured in the laboratory after transport from the field,[24] were: bulk density = 1.87 g/cm^3, water content = 10.31%, and freezing temperature = −0.2°C. The sand is fine-grained (Table 1).

Soil specimens in this study comprise remolded samples. Following the industrial standard of the People's Republic of China,[25] sand was dried in an oven at 105°C for 48 h. The dry sand was then mixed with a specific amount of water to achieve the required uniform water content. Next, loose moist sand was compacted into a PVC pipe (72 mm high and 85 mm in diameter) to meet the required uniform density. Sand temperature was measured by cylindrical platinum resistance thermometers (Pt100) manufactured by Heraeus Co Ltd. The Pt100 temperature sensors (diameter 4 mm and length 15 mm) were calibrated to an accuracy of ±0.1°C in an ice–water bath, then embedded in the specimens at heights of 35, 45, 55 and 70 mm above the base (Figure 1a). Finally, rubber insulation (30 mm thick) was wrapped around each specimen, except for the bottom, to minimize the influence of external temperature.

2.2 | Monitoring strategy

Our monitoring strategy relied on instrumenting sand samples with Pt100 temperature sensor arrays and a nonmetal ultrasonic measuring system, NM-4A (manufactured by KangKeRui Ultrasonic Engineering Co., Ltd). This allowed us to measure temperature and acoustic parameters at different stages of freezing, as the cryofront ascended to specific heights above the base of the specimens.

Ultrasonic testing during freezing involved four steps. First, the ultrasonic apparatus was calibrated before measurement[26] to calculate the inherent time delay t_0. A thin film of petroleum jelly was used to ensure good acoustical coupling between the sand

TABLE 1 Grain-size fractions of fine sand

Grain diameter (μm)	>250	250–225	225–200	200–175	175–150	150–125	125–100	100–75	75–50
Percentage	0.59	19.86	26.72	11.75	18.56	11.42	5.78	3.69	1.63

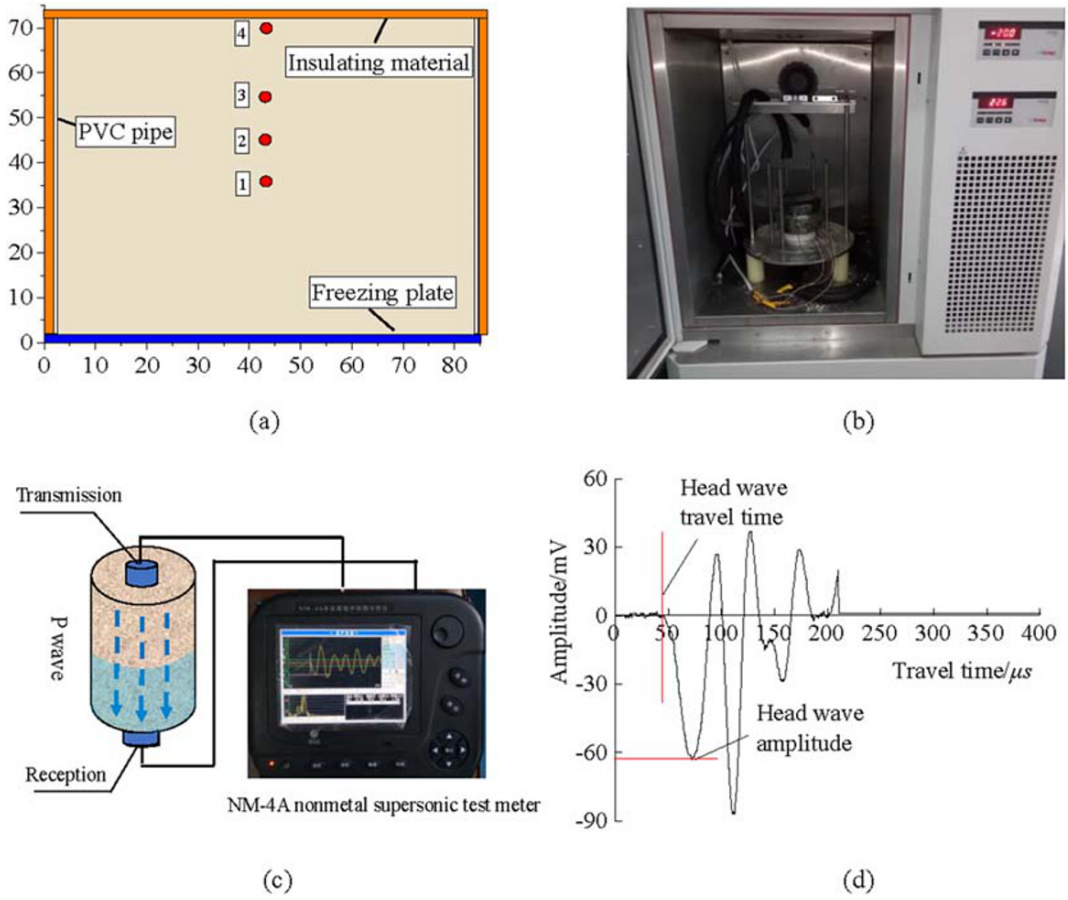

FIGURE 1 Experimental system of partial freezing. (a) Vertical cross-section of sand specimen showing location of four Pt100s (red circles); all units are in millimeters. (b) XT5405B frost-heave instrument. (c) Schematic diagram showing frozen lower part of specimen (blue) and unfrozen upper part (brown) and location of ultrasonic sensors. (d) Example of waveform of receiving ultrasonic wave [Colour figure can be viewed at wileyonlinelibrary.com]

sample and acoustic transducers and to eliminate any air pockets between them. The apparatus was then used to measure freezing of the sand specimen in a DWB thermostatically controlled tank, which can provide constant temperatures from −40 to 30°C, based on the arrival time of the cryofront at specific heights. Next, an ultrasonic wave propagated through the sample and acoustic parameters were recorded. Finally, acoustic parameters were calculated, including wave velocity, wave amplitude, and frequency spectrum based on ultrasonic theories.[27,28]

The gravimetric water content of the sand was measured when the cryofront had reached four specified heights (35, 45, 55 and 70 mm) to determine water migration. At each height, one specimen of soil was divided into horizontal subsamples 1 cm thick. Unfrozen soil was sampled from the PVC pipe with a soil sampler geotome, and underlying frozen soil was sampled with a knife. Each subsample was weighed, dried in an oven (105°C) for 24 h, reweighed and the moisture content was calculated. Overall, the moisture content was determined from four soil specimens for each of three water contents (7.31, 10.31, and 13.31%), giving a total of 12 specimens.

2.3 | Experimental system and procedure

Progressive upward freezing experiments were performed on sand specimens at three different water contents (7.31, 10.31, and 13.31%), which represent three degrees of saturation (54.03, 76.2, and 98.38%) and a single density (1.87 g/cm^3) and temperature of basal cold plate (−20°C). The experiments were carried out in the Deep Coal Mine Construction Technology Laboratory of the National Engineering Laboratory of China.

The testing system included a frost heave instrument, an ultrasonic detector and an ultrasonic transducer (50 kHz) (Figure 1). The

frost heave instrument (XT5405B) consisted of a thermostat, cold plate, and refrigerant circulation unit, which can provide temperatures from −40 to 40°C (manufactured by Xutemp Temptech Co. Ltd). The temperature of the cold plate was measured by a thermocouple inside the instrument and its precision was ±0.02°C. The basal cold plate enabled upward freezing of the sand specimens.

The nonmetal ultrasonic detector (NM-4A) consisted of four units: (a) one emission and one receiving transducer, (b) a pulse-receiver, (c) a waveform measuring system, and (d) 3 m of wire. Its launch voltage range was 250–1,000 V, the measurement accuracy of sound-intervals was ±0.05 μs, the receiver sensitivity was ≤10 μV, the amplitude range was 0–177 dB, and the range of amplifier bandwidth was 5–500 kHz. The ultrasonic transducers have a mean frequency response of 50 kHz, and the waveform of the excitation is a sine wave.[21] The sampling interval was 0.4 μs, the launch voltage was 500 V, and the number of sample measurements was 1,024 at each time of ultrasonic testing.[22]

The experimental procedure is summarized in a flowchart with seven stages (Figure 2). (1) The wetted and remolded sand specimens were compacted into a PVC pipe, as described above, and placed on the basal freezing plate. (2) The unfrozen specimens were measured by ultrasonic testing according to the mechanical industrial standard of the People's Republic of China JB/T 8428-2015, and acoustic parameters of sand samples at different water content were recorded. (3) The acoustic parameters (wave velocity, head wave amplitude, and frequency spectrum) of unfrozen samples at three water contents were compared. (4) The specimens were frozen progressively from the base upwards and sand temperature was measured at 5-s intervals. (5) Ultrasonic parameters were measured immediately after the cryofront arrived at specified heights (35, 45, 55, 70 mm). (6) The moisture content of the frozen and unfrozen sand was measured in 1-cm vertical increments. (7) The variation of wave velocity, amplitude, and frequency spectrum at different freezing periods was compared and analyzed.

2.4 | Ultrasonic parameters

The ultrasonic parameters determined in this study are wave velocity, head wave amplitude, and frequency spectrum. The velocity of compressional and shear waves indicates the physical properties of frozen soil and can be measured directly in the laboratory (e.g., [16,17]). The compressional wave (p wave) velocity was the main acoustic parameter measured in this study because it is easier to obtain than shear wave velocity under field conditions. The p wave velocity (V_p, km/s) is expressed as:

$$V_p = \frac{L}{t_p - t_0} \tag{1}$$

where L is the length of the specimen (mm), t_p is the travel time of the first wave in frozen soil (μs), and t_0 is the inherent time delay (μs).

The head wave (i.e., first wave) amplitude (A_h) represents the energy magnitude of the head receiving wave and can be recorded automatically by a supersonic test meter.[21] Changes in transmitted amplitude show the variation in contact area between soil particles and can be used to estimate the amount of compaction, changes in void ratio, and associated changes in normal stress (e.g., [29–31]). An increase in contact area between the particles leads to an increase in values of transmitted amplitude through the soil specimen.[31]

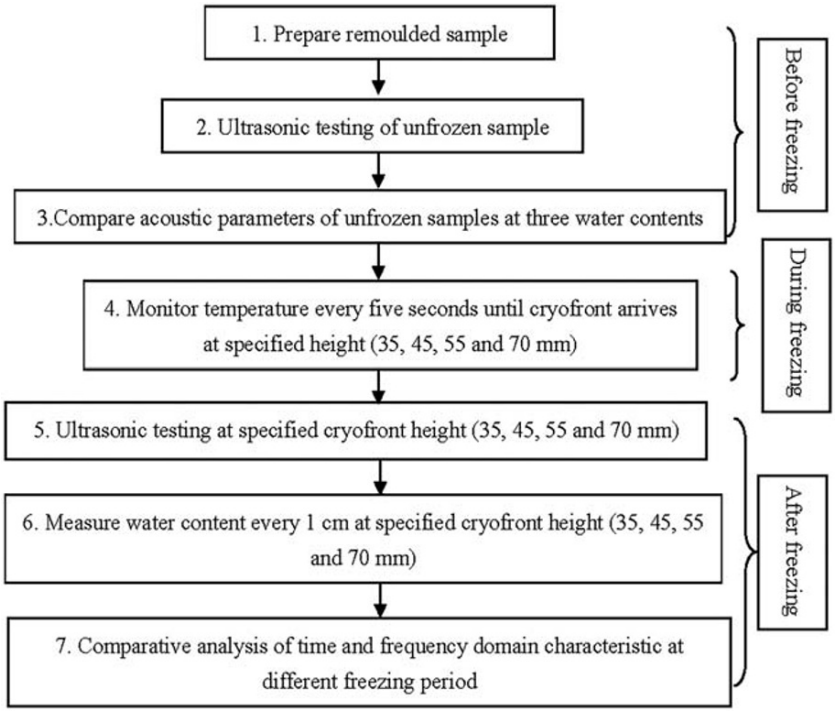

FIGURE 2 Flowchart showing the stages in the experimental procedure

The frequency spectrum can be calculated by a fast Fourier transform (FFT), which converts data from the time domain into the frequency domain of waveforms (e.g., [32–36]). The frequency spectrum of receiving ultrasonic waves relates to the changes in volume and distribution of inter-particle pores in a soil.[21] Pyrak-Nolte et al.[37] found that fractures and flaws filter the high-frequency content of the transmitted wave. Therefore, the frequency spectrum can determine whether particular frequency components are present in the analyzed signal at different freezing periods, because water migration during progressive upward freezing can lead to variation in the distribution of inter-particle pores.

A wavelet transform was used to eliminate high-frequency noise signals from the original signals and to improve the signal characteristics substantially, because ultrasonic waves are nonstable and transient (e.g., [21,38,39]). The db5 wavelet was selected to disassemble the receiving wave signals into five levels. After wavelet transformation, with the cutoff frequency set at 100 kHz, the reconstructed effective signals were processed by an FFT, to obtain the distribution of the frequency spectrum of fine sand at different stages during progressive upward freezing.

3 | RESULTS AND ANALYSIS

3.1 | Temperature profiles

The vertical temperature profiles and cryofront positions in the sand specimens at three water contents during four different stages of upward freezing are shown in Figure 3. The temperature of the freezing plate was kept at −20°C to meet the typical temperature boundary conditions of artificial ground freezing. When the cryofront reached heights of 35–45 mm (Figure 3a, b), the temperature in the unfrozen sand tended to decrease faster in samples at lower water content (7.31%) than it did in those at higher water content (10.31 and 13.31%). This is because increasing water contents lead to increases in specific heat capacity, resulting in greater resistance to temperature change in the unfrozen section. In contrast, the temperature was almost the same in the frozen section. As the cryofront rose through the specimens, the average temperature of the frozen section decreased significantly. The reason for the observed changes is that the thermal conductivity of frozen soil exceeds that of unfrozen soil and the specific heat capacity of frozen soil is lower

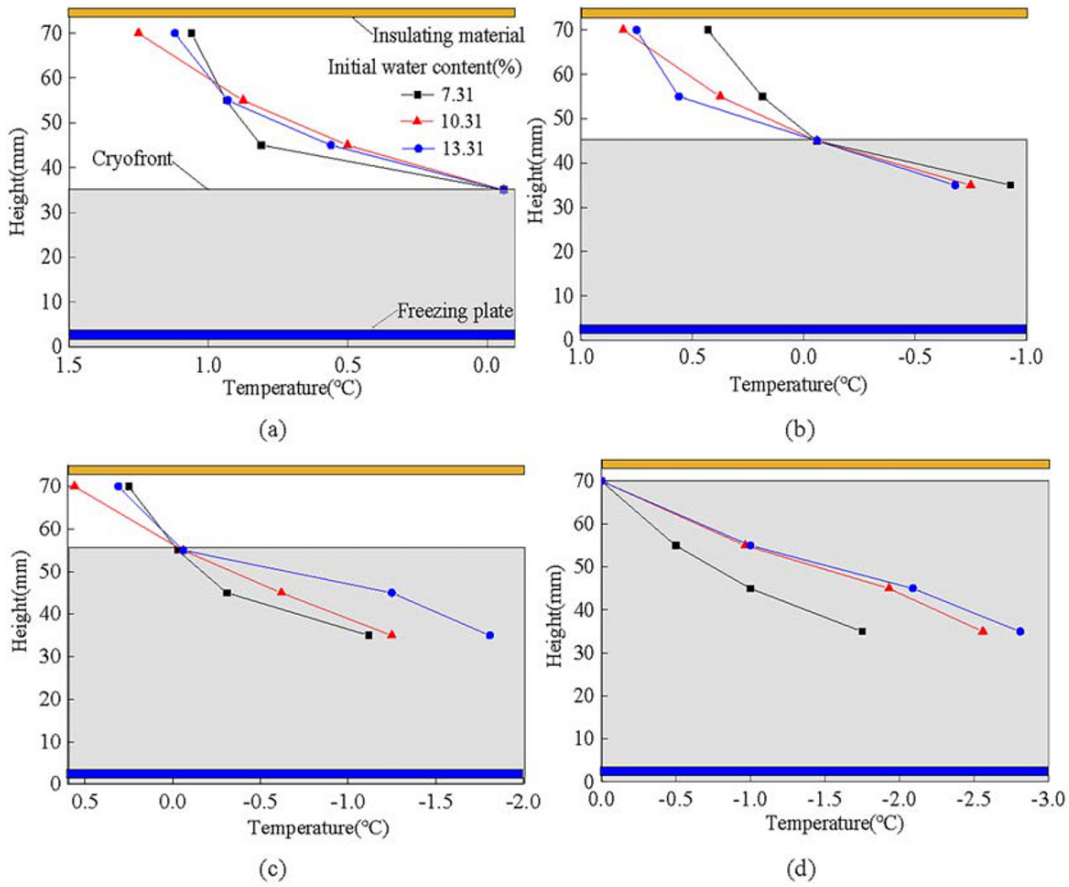

FIGURE 3 Vertical profiles of temperature in specimens at three different water contents during upward freezing when the cryofront reached heights of (a) 35 mm, (b) 45 mm, (c) 55 mm, and (d) 70 mm. Gray area indicates frozen sand and white area indicates unfrozen sand [Colour figure can be viewed at wileyonlinelibrary.com]

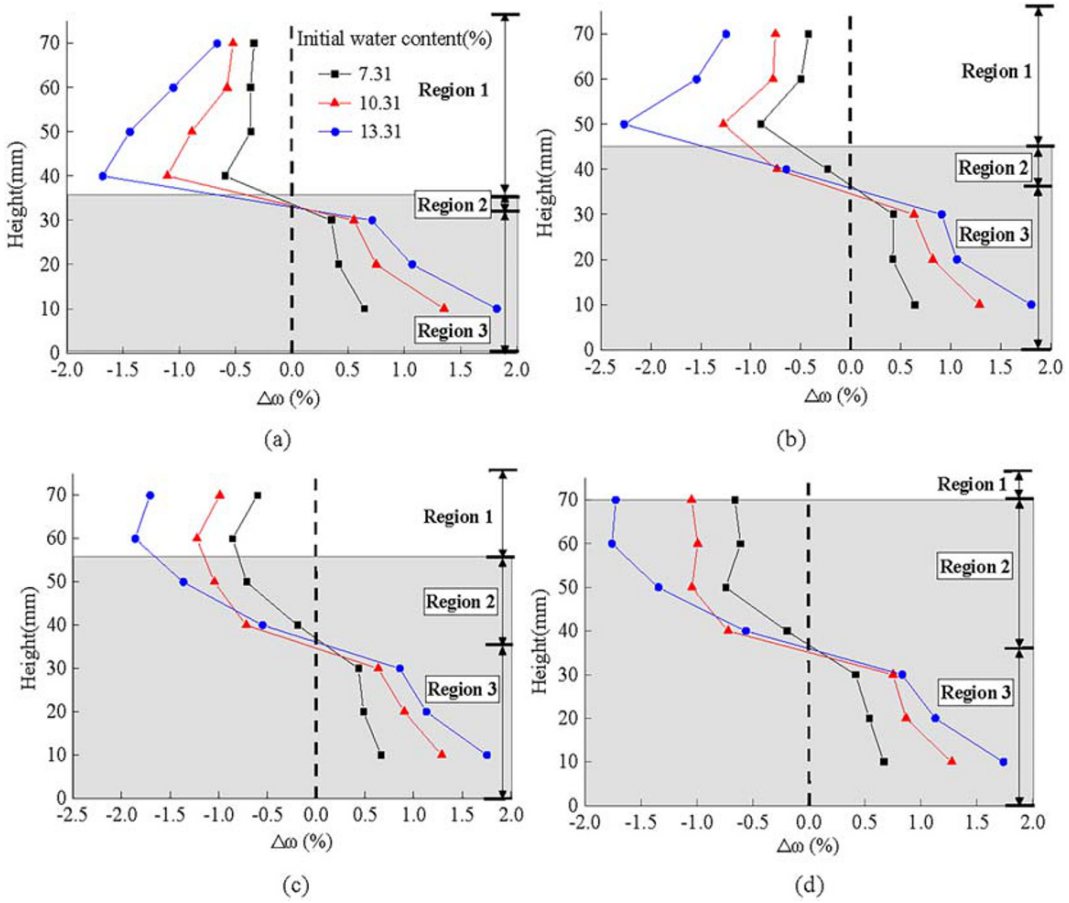

FIGURE 4 Vertical profiles of water content change—relative to the dashed vertical line—through sand specimens when the cryofront reached heights of (a) 35 mm, (b) 45 mm, (c) 55 mm, and (d) 70 mm. Initial water contents are indicated. Gray area indicates frozen sand and white area indicates unfrozen sand. Regions 1–3 are illustrated in Figure 5 [Colour figure can be viewed at wileyonlinelibrary.com]

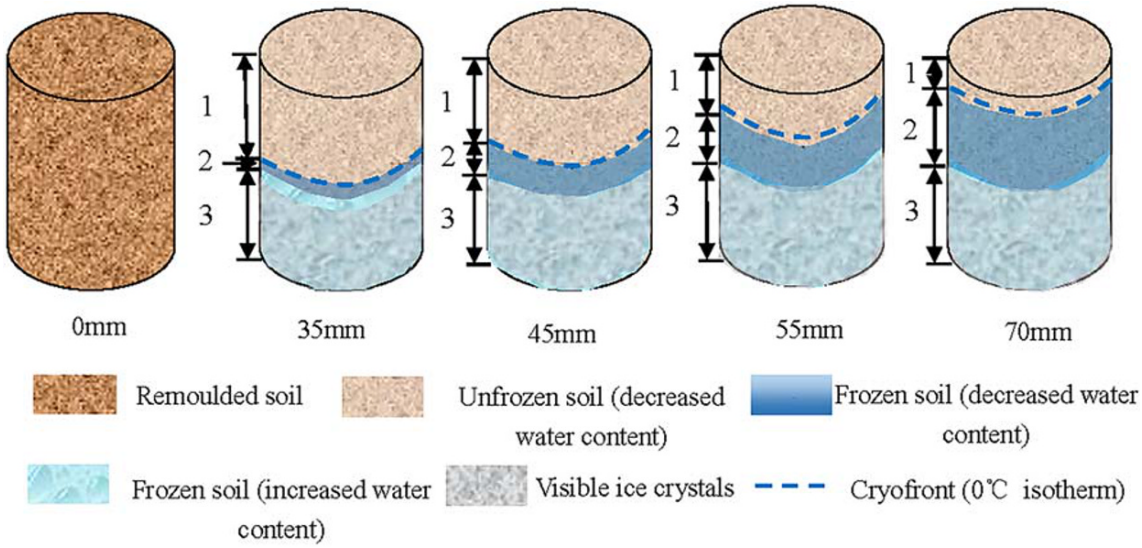

FIGURE 5 Different regions of the specimen during upward freezing. Units are in millimeters [Colour figure can be viewed at wileyonlinelibrary.com]

than that of unfrozen soil. Because thermal conductivity is inversely proportional to the temperature of frozen soil, temperature decreased as water content increased when the cryofront reached 70 mm height.

3.2 | Changes in water content

Vertical profiles of water content change ($\Delta\omega$) in the sand specimens during upward freezing are presented in Figure 4. The change is shown relative to initially uniform vertical profiles (normalized to 0% in Figure 4) at three different starting water contents during four stages of upward freezing. Both increases and decreases in water content characterized different parts of the frozen section, whereas decreases characterized all of the unfrozen portion, with the greatest decreases in the unfrozen sand directly above the cryofront. The frozen section of increased water content was stable at around 35 mm height, whereas the section of decreased water content spread upwards as the cryofront ascended from 35 to 70 mm height (Figure 4). The trend of water migration weakened gradually as the cryofront approached and reached 70 mm height (Figure 4) in the unfrozen section. In summary, water in all samples migrated through the unfrozen section and into the frozen section (i.e., in the same direction as the temperature gradient; Figure 4).

Three evolving regions in the sand specimens developed during upward freezing and can be distinguished from top to bottom of the specimens (Figure 5).

1. *Unfrozen sand with decreased water content*. In region 1, the mass of water declined more in specimens with higher initial water content. For example, maximum declines of 0.856, 1.224, and 1.856% were determined for initial water contents of 7.31, 10.31, and 13.31%, respectively, when the cryofront reached 55 mm height.
2. *Frozen sand with decreased water content*. In region 2, the temperature was below 0°C and the mass of water was less than that of the initial water content. The maximum decreases in water content for different initial moisture contents (7.31, 10.31, and 13.31%) were 0.742, 1.048, and 1.758%, respectively, when the cryofront was around 70 mm height. The vertical thickness of region 2 increased as the cryofront rose from 35 to 70 mm, with a maximum value of 35 mm when the cryofront reached 70 mm (Figure 4d). Much of region 2 was ice-cemented, except for the uppermost ~5 mm.
3. *Frozen sand with increased water content*. In region 3, the temperature was below 0°C and the mass of water was more than that of the initial water content. Increases in moisture content were greater for specimens with initially greater water contents. The average temperature of region 3 was distinctly lower than that of region 2 and the mass of water increased gradually with depth. Ice crystals were visible in almost all of region 3 during freezing. The crystals were up to a few millimeters in length or diameter (Figure 6).

FIGURE 6 Visible ice crystals (white) in region 3 (ice-rich zone) when the cryofront reached a height of 35 mm. Scale in millimeters [Colour figure can be viewed at wileyonlinelibrary.com]

3.3 | Ultrasonic time-domain characteristics

Under normal circumstances ultrasonic receiving waves show a spindle waveform (He et al., 2007), but wave period reduction and messy receiving waves appear when ultrasonic waves are transmitted through soil with high porosity or other defects. The receiving waveforms in fine sand at different water contents and stages of upward freezing are shown in Figure 7. The receiving waveforms of fine sand change during freezing, because of the variation of temperature and water migration. The vertical red line in Figure 7(a) indicates the arrival time of the head wave, whereas the horizontal red line indicates the amplitude of this wave.

In unfrozen sand, the receiving wave had only one wave period and the waveforms were loose (Figure 7a). This indicates that scattering attenuation of ultrasonic waves occurred during wave transmission, because unfrozen fine sand has low bulk and shear stiffnesses and a high void ratio. The receiving wave reduced to a half cycle as the height of the cryofront increased to 35–45 mm (Figure 7b–c), which indicates greater scattering attenuation, mainly because the air content increased while the water content decreased in the unfrozen region 1. As ice crystals grew, the contact area between soil particles increased, and this is thought to explain the increase in wave energy in the frozen regions 2 and 3. This function can almost be ignored relative to the increasing scattering attenuation in the unfrozen region 1 when the cryofront reached 35–45 mm. When the cryofront ascended to 55 mm height, the number of receiving wave cycles in sand at initial water contents of 7.31% and 10.31% increased substantially (Figure 7d). This demonstrates that the increase of wave energy in the frozen regions 2 and 3 was higher than the decrease of scattering attenuation in the unfrozen region 1 at this stage of freezing.[40] All receiving wave cycles showed multiple cycles when the cryofront reached the top of the specimen (Figure 7e).

The compressional wave (p wave) velocity (V_p) was recorded automatically according to Equation 1. As shown in Figure 8(a), V_p increased slowly before the cryofront reached a height of 35 mm and then increased substantially when the cryofront rose to 55 mm. Thereafter, the growth rate dropped as the cryofront approached the

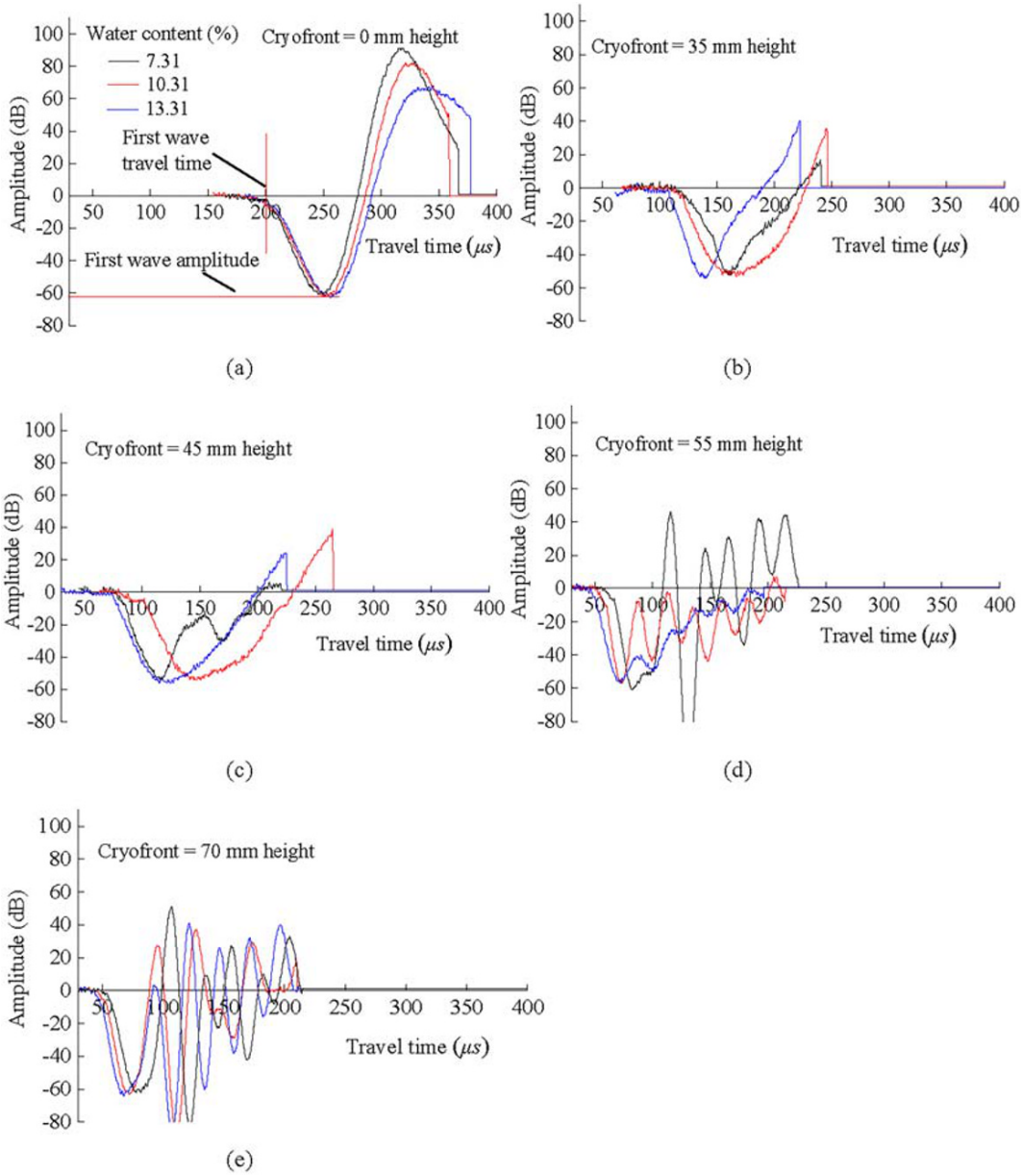

FIGURE 7 Receiving waveform of fine sand specimen during upward freezing as the cryofront reached heights of (a) 0 mm, (b) 35 mm, (c) 45 mm, (d) 55 mm, and (e) 70 mm. Note variation in scale of vertical and horizontal axes [Colour figure can be viewed at wileyonlinelibrary.com]

top of the specimen. The values of V_p were similar before the cryofront arrived at 45 mm and became higher for specimens with higher water content during later stages of freezing.

During early stages of freezing (0–35 mm height of the cryofront), the p-wave velocity between the three specimens was similar to each other. The main reason for this is that large parts of the specimens were unfrozen and contained substantial amounts of air, which limits the p-wave velocity.

During middle stages of freezing (cryofront at 35–55 mm height), about half to more than half of the sample was frozen as the cryofront rose (Figure 5), and the rate of increase of wave velocity was greatest (Figure 8a). At this time, the volume of unfrozen sand decreased rapidly while the volume of frozen sand increased rapidly, which explains the changes of wave velocity.

During later stages of freezing (cryofront at 55–70 mm height), much of sample was frozen, and therefore the rate of increase in wave velocity decreased (Figure 8a). In addition, the bulk, shear modulus, and strength of frozen soil is higher with higher water content in the frozen regions 2 and 3.[16] Thus, when the cryofront arrived at 55 mm and 70 mm height, the wave velocity in the specimen with an initial water content of 13.31% was distinctly greater than that of 10.31%, which in turn exceeded that of 7.31%.

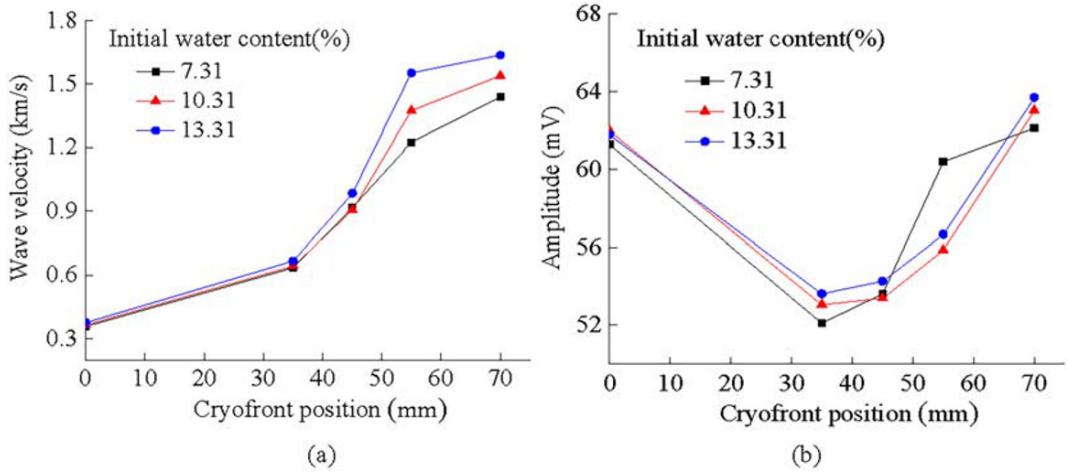

FIGURE 8 The p-wave velocity (a) and head wave amplitude (b) of fine sand during upward freezing [Colour figure can be viewed at wileyonlinelibrary.com]

Overall, wave velocity increased continually as the cryofront rose through the specimens, indicating that measurements of wave velocity can reveal the cryofront position during upward freezing.

The head wave amplitude showed a parabolic relationship with increasing cryofront height (Figure 8b). During early stages of freezing (cryofront lower than 35 mm), an increase in cryofront height was associated with a decrease in wave amplitude, whereas during later stages (35–55 mm) the amplitude increased gradually. Eventually the absolute values of wave amplitude exceeded initial values. The increase of the volume of the ice-cemented section (regions 2 and 3) led to an increased contact area between the sand particles because ice crystals occupied more of the pore volume and formed new inter-particle contact areas in frozen sections. However, the reduction of water in the unfrozen section resulted in more air among the sand grains and less inter-particle contact area. Therefore, a change of wave amplitude indicates that the function of unfrozen section is greater than the frozen section during most of the freezing period. In summary, wave amplitude decreased during early stages of freezing and increased during later stages, which indicates that wave amplitude cannot be used as a method to calculate the cryofront position during upward freezing.

3.4 | Ultrasonic frequency-domain characteristics

The distribution of the frequency spectrum during upward freezing was obtained by FFT after wavelet transform (Section 2.4) and is summarized in Figure 9. The morphology of the frequency spectrum varied progressively during different stages of upward freezing. Early stages of freezing (0–35 mm height of the cryofront) were characterized by a frequency spectrum with a single peak, whereas during later stages (35–70 mm height) the frequency spectrum became more irregular and multi-peaked. The multi-peak frequency spectrum shows the frequency of three regions (Section 3.2).

The lowest frequency value (2.44 kHz)—indicated by the number 1 in Figure 9(e)—is less than that of the original, unfrozen remolded soil (4.88 Hz). The former value developed during every freezing period, which indicates that the frequency of region 1 (unfrozen sand with a decreased water content; see Figure 5) is 2.44 kHz.

Intermediate frequency values (19.53–26.86 kHz)—indicated by the number 2 in Figure 9(e)—varied with water content and cryofront height. The higher frequency components only developed after the cryofront reached 55 mm height. The drier specimen (7.31% water content) showed higher frequency components much earlier than the two wetter specimens (10.31 and 13.31%). These findings indicate that the higher frequency components of ultrasonic signals were absorbed before the cryofront reached 55 mm height, and then they appeared gradually due to decreased scattering attenuation in region 1 (Figure 5) with the increase of cryofront height. The intermediate values can be considered as the frequency of region 2 (frozen sand with decreased water content).

The highest frequency components (39.06–50 kHz)—indicated by the number 3 in Figure 9(e)—also developed after the cryofront reached 55 mm height. Again, the driest specimen (7.31% water content) showed the highest frequency components much earlier than the two wetter ones (10.31 and 13.31%). The highest frequency components can be regarded as the frequency of region 3 (frozen sand with increased water content), and the range of 39.06–50 kHz is close to that of frozen fine sand.

In summary, the frequency components during the later stages of upward freezing can reveal the frequency of different frozen and unfrozen regions due to phase change and water migration. However, the dominant frequency of the specimen cannot be used to evaluate the freezing state because the maximum amplitude in the frequency spectrum (i.e., dominant frequency) is always 2.44 kHz during progressive upward freezing.

As the cryofront ascended, the height of three evolving regions changed, thus affecting the frequency distribution due to the frequency-selecting property of wave-absorption. To analyze

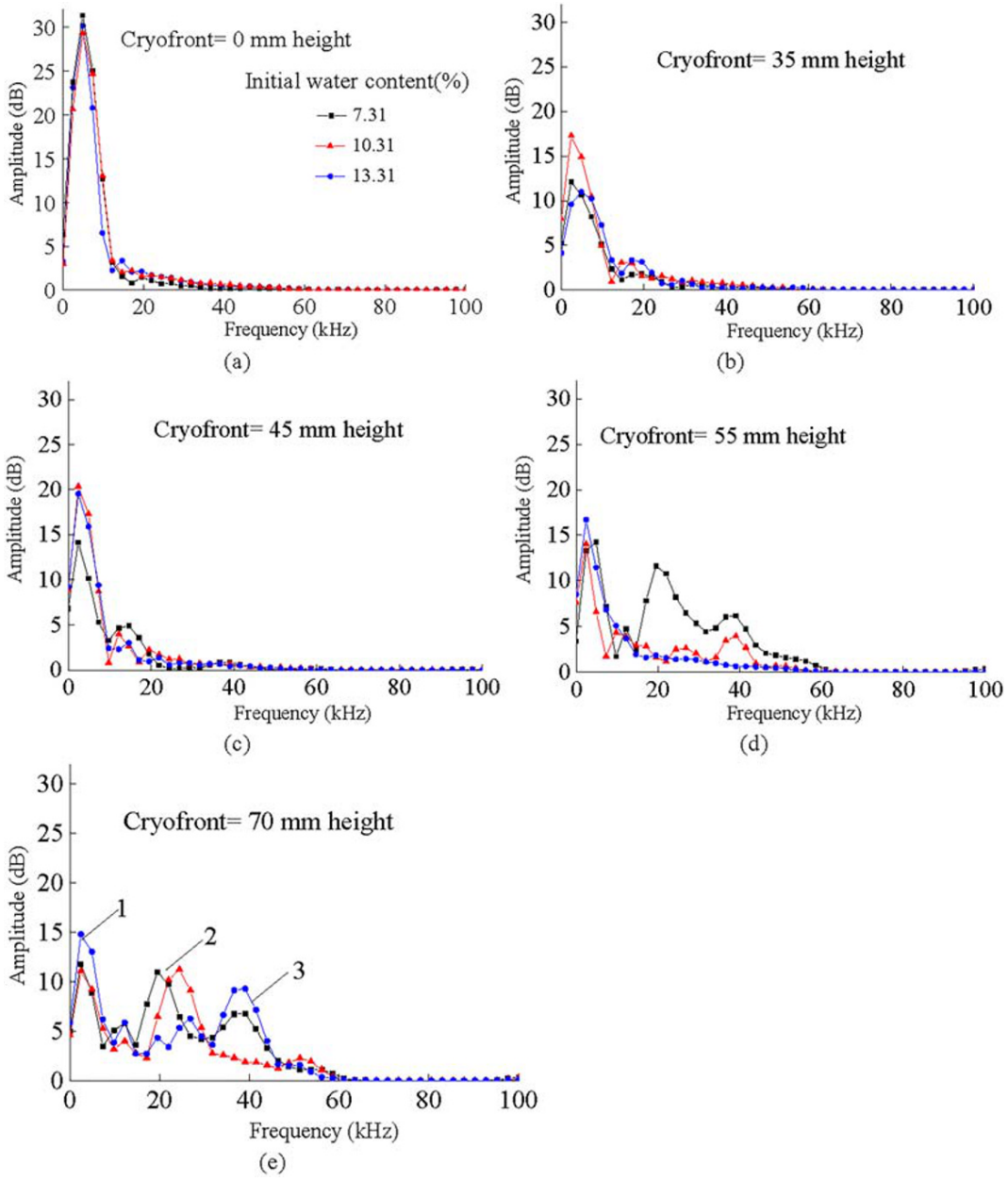

FIGURE 9 Receiving frequency spectrum of fine sand specimen during upward freezing. Cryofront is shown at heights of (a) 0 mm, (b) 35 mm, (c) 45 mm, (d) 55 mm, and (e) 70 mm [Colour figure can be viewed at wileyonlinelibrary.com]

quantitatively the ultrasonic frequency-domain characteristics of fine sand during upward freezing, the values of the kurtosis of the frequency spectrum (KFS) were calculated.[21] Kurtosis is a statistical measure of th e "peakedness" of a distribution[41]: the more irregular and multi-peaked a distribution is, the lower the value of KFS. KFS was calculated as follows:

$$KFS = \frac{\sum_{i=0}^{N} A_i(\ f_i - f_p)^4}{\left(\sum_{i=0}^{N} A_i(\ f_i - f_p)^2\right)^2} \quad (2)$$

where f_i and f_p are the values of discrete frequency and peak frequency, respectively (kHz), and A_i is the discrete frequency amplitude (db).

As shown in Figure 10, the value of KFS gradually decreased during the later stages of upward freezing (55–70 mm) and reached the minimum value when the cryofront arrived at the top of the sample. Clearly, the KFS values of the three water contents during early stages of freezing (0–55 mm) were higher than during later freezing stages (55–70 mm), and the minimum value of KFS was almost equal (0.01989–0.03179) when the cryofront arrived at the top of the sample.

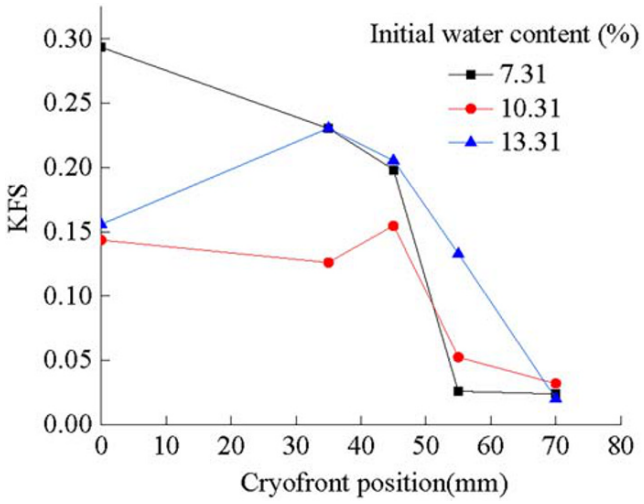

FIGURE 10 The kurtosis of frequency spectrum (KFS) of fine sand specimen during upward freezing [Colour figure can be viewed at wileyonlinelibrary.com]

4 | DISCUSSION

4.1 | Identifying the freezing state of progressively frozen sand

4.1.1 | Single vs multiple peaks and KFS change in the frequency spectrum

As illustrated in Section 3.4, a multiple-peak frequency spectrum only characterized progressively frozen sand and the KFS value was lower during later stages of upward freezing (55–70 mm height of the cryofront) than during early stages, whereas a single-peak frequency spectrum characterized unfrozen and progressively frozen sand during the early stage of freezing (0–45 mm height). Therefore, during later stages of freezing, a single-peak frequency spectrum or KFS value that is higher than during early stages is abnormal and indicates that the cryofront moved slowly, which may be caused by cold source shortage or limited heat transfer. In addition, a multiple-peak frequency spectrum or a KFS value that is very low during early stages of freezing is abnormal, which indicates that the cryofront has moved faster than normal, which may be caused by lower initial temperature or low source temperature. More generally, single-peak and multiple-peak frequency spectra and KFS values could be used as evaluation methods to identify the freezing state of progressively frozen sand.

Our laboratory results can be compared with field observations obtained during artificial ground freezing engineering at Baiyun Airport, Guangzhou, China, where the average depth of the groundwater table was 4.37 m. As shown in Figure 11, the frozen soil at 16 m depth was measured by the ultrasonic wave transmission method, with a distance between inspection holes J_1 and J_2 of 1.47 m. Two cylindrical transducers (one emission, the other reception) were placed at the same depth (−16 m) in the inspection holes. Brine was used to ensure good acoustical coupling between the sides of each hole and the transducers. A launch voltage of 1,000 V and sampling period of 1.6 μs were selected. Wave velocity were measured by ultrasonic testing during different stages of freezing (0, 24, 26, 42, and 60 days).

The trend of the receiving frequency spectrum of fine sand measured in the field (Figure 12a) is similar to that measured in the laboratory (Figure 9). The frequency spectrum of undisturbed sand in the field is a single peak. During the earlier stages of freezing (0–24 days), the dominant frequency was slightly lower than that of undisturbed soil. The morphology of the frequency spectrum became multi-peaked during later stages of freezing (24–60 days). Therefore, the gradual change from a single-peak frequency spectrum to a multiple-peak one can demonstrate that the frozen wall developed normally.

The trend of KFS of fine sand calculated in the field (Figure 12b) is similar to that calculated in the laboratory (Figure 10). KFS decreased gradually as freezing time increased, and the minimum value of KFS is 0.0883 when the cryofront arrived at J_2 (60 days).

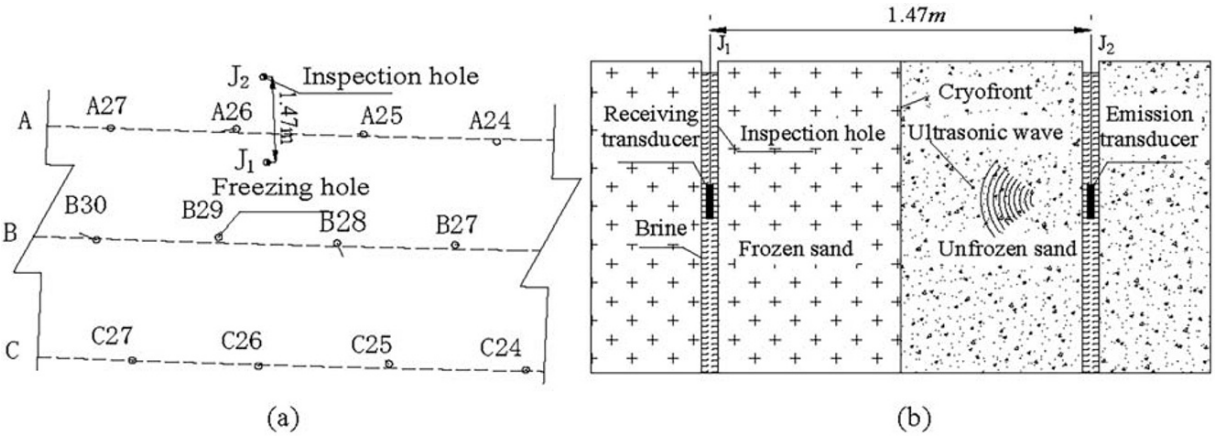

FIGURE 11 Arrangement of freezing holes and sensors for field observations: (a) plan view showing location of freezing holes and (b) vertical profile showing location of ultrasonic sensors

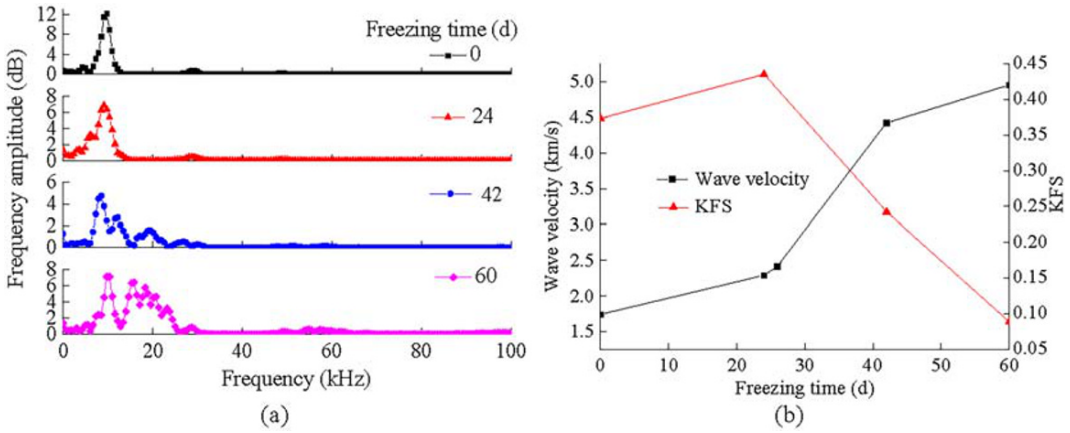

FIGURE 12 Receiving frequency spectrum (a) and wave velocity and KFS (b) of fine sand measured at different times of freezing in the field [Colour figure can be viewed at wileyonlinelibrary.com]

However, when the cryofront arrived at J_2 (Figure 11) the frequency components of the field results are more complex and KFS is higher than laboratory results. The main reason for this is that underground water continually supplies water into unfrozen soil in the field, whereas such water supply was absent in the laboratory.

4.1.2 | Variation of wave velocity

The trend of wave velocity of progressively frozen fine sand measured in the field is also similar to that of wave velocity measured in the laboratory (Figure 12b). The rate of increase of V_p during the early stages of freezing (0–24 days) is lower than that during middle stages (24–42 days). During later stages of freezing (42–60 days), the rate of increase of V_p decreases. The wave velocity value measured in the field is higher than that in the laboratory, mainly because formation pressure had compacted the frozen soil in the field, whereas frozen soil was measured under unloaded conditions in the laboratory. Therefore, if lower wave velocity is measured during later stages of freezing, especially if the measured value is similar to that of undisturbed soil, it can be considered to indicate an abnormal freezing state that reflects the slow movement of a cryofront.

4.2 | Calculation of frozen section thickness

4.2.1 | Frozen section thickness of laboratory test

As shown in Figure 13, the specimen that was progressive frozen in the laboratory can be divided into frozen and unfrozen sections according to the cryofront position because the partially frozen layer (temperature range: −0.2 to 0°C) in progressively frozen sand is so thin that it has little impact on the accuracy of the calculation of frozen section thickness. The total travel time of the head wave in the specimen τ_p (μs) can be expressed as:

$$\tau_p = \frac{S_f}{v_f} + \frac{S - S_f}{v_u} \tag{3}$$

where S is the length of the specimen (mm), S_f is the thickness of the frozen section (mm), v_f is the average wave velocity of the frozen section (km/s) and v_u is the average wave velocity of the unfrozen section (km/s).

By rearranging Equation 3, we obtain the value of the frozen section thickness as:

$$S_f = v_f \frac{S - \tau_p v_f}{v_f - v_u} \tag{4}$$

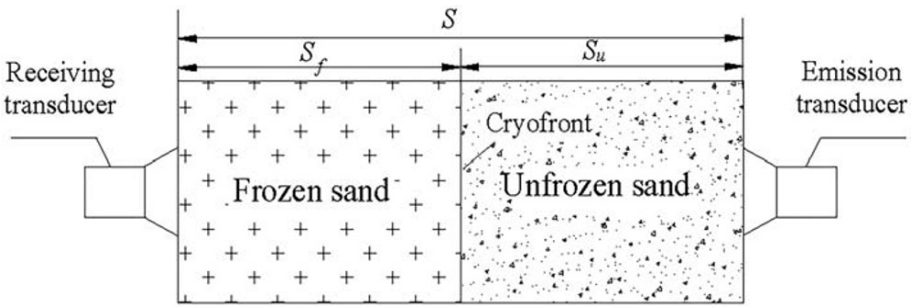

FIGURE 13 Sketch of horizontal cross-section through frozen and unfrozen sand showing detection of frozen sand thickness by ultrasonic wave testing

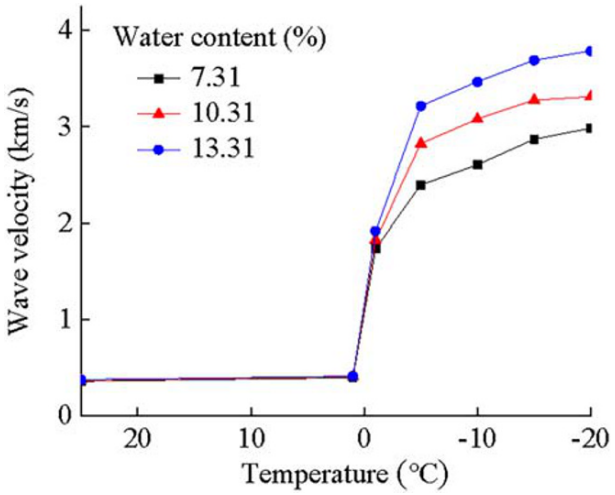

FIGURE 14 Wave velocity versus temperature at different water contents under constant temperature [Colour figure can be viewed at wileyonlinelibrary.com]

The average wave velocity through the frozen and unfrozen sections changes continually as freezing progresses, both in the field and in the laboratory. Thus, v_f and v_u are difficult to determine accurately during progressive freezing.

The relationship between wave velocity and temperature of fine sand at different water contents under constant temperature was measured in the laboratory (Figure 14).[23] Wave velocity increases slightly as temperature decreases before fine sand freezes. Therefore, the average wave velocity of the unfrozen section v_u can be treated as the wave velocity of undisturbed soil, which can be measured before freezing. However, wave velocity increases sharply as temperature decreases below 0°C, which demonstrates that the average wave velocity of the frozen section v_f changes significantly during progressive freezing.

Three parameters in Equation 4—S, τ_p, and v_u—can be measured easily in the laboratory. Based on our experimental results, S is 72 mm, v_u values of specimens with different water contents (7.31, 10.31, and 13.31%) are 0.358, 0.365, and 0.376 km/s, respectively,

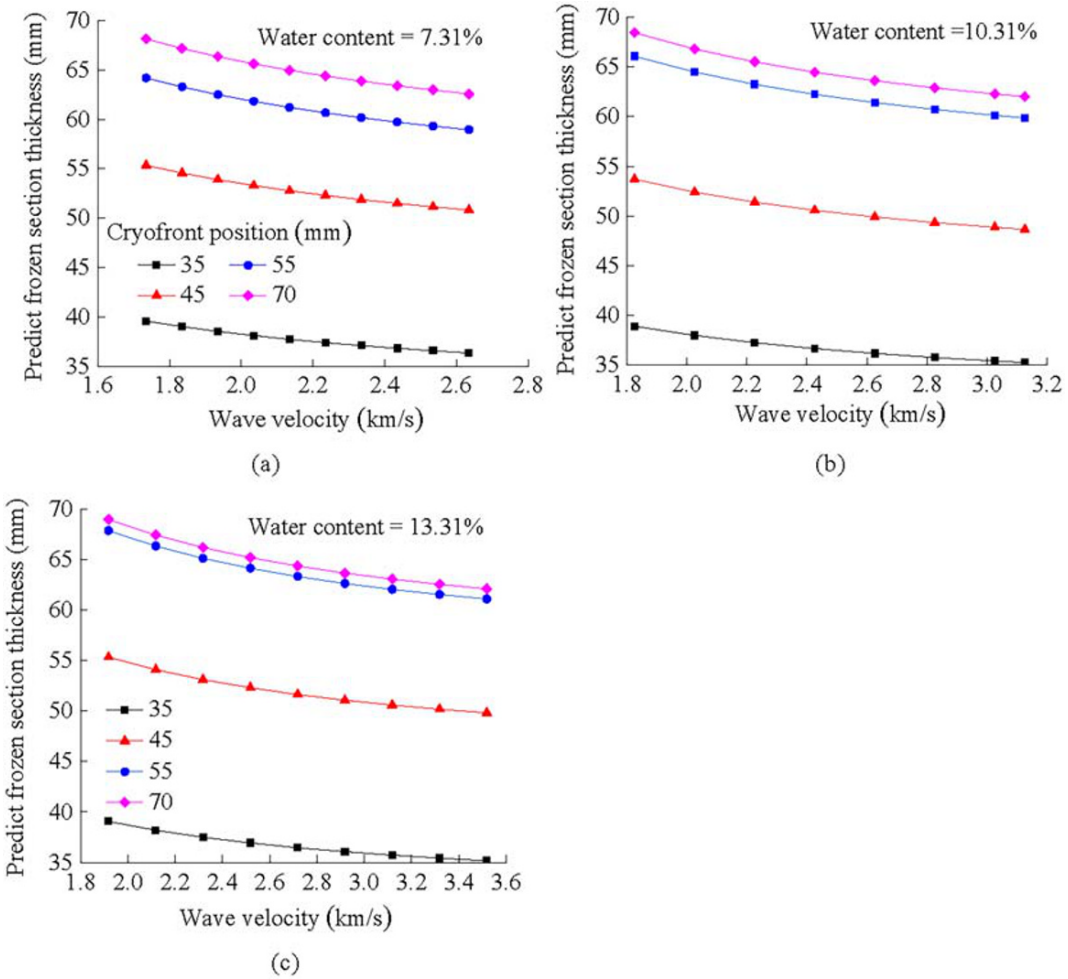

FIGURE 15 Predicted thickness of frozen fine sand when v_u is wave velocity of undisturbed soil: specimens with water content of (a) 7.31%, (b) 10.31%, and (c) 13.31% [Colour figure can be viewed at wileyonlinelibrary.com]

TABLE 2 Predicted and measured values of frozen section thickness

Water content (%)	Length (mm)	Travel time (μs)	v_u (km/s)	v_f (km/s)	Predicted value (mm)	Measured value (mm)	Accuracy (%)
7.31	72	113.386	0.358	2.604	36.41	35	95.96
	72	78.431	0.358	2.604	50.92	45	86.84
	72	58.824	0.358	2.604	59.06	55	92.62
	72	50.070	0.358	2.604	62.69	70	89.56
10.31	72	111.975	0.365	3.079	35.32	35	99.10
	72	79.558	0.365	3.079	48.74	45	91.69
	72	52.402	0.365	3.079	59.98	55	90.94
	72	47.213	0.365	3.079	62.13	70	88.76
13.31	72	107.946	0.376	3.465	35.24	35	99.33
	72	73.171	0.376	3.465	49.90	45	89.10
	72	46.392	0.376	3.465	61.20	55	88.73
	72	44.010	0.376	3.465	62.20	70	88.86

TABLE 3 Parameters relating to predicted and measured values of frozen wall thickness

Freezing period (days)	Distance (mm)	Travel time (us)	v_u (km/s)	v_f (km/s)	Predicted value (mm)	Measured value (mm)	Accuracy (%)
24	1,470	642.33	1.741	4.884	547.35	605	90.32
26	1,470	609.16	1.741	4.884	637.44	660	96.54
42	1,470	332.53	1.741	4.884	1,384.73	1,413	98.03

similar to values from undisturbed soil, and τ_p is a measured value at different freezing periods. The relationship between predicted frozen section thickness S_f and v_f (Figure 15) is based on inputting values of S, τ_p and v_u into Equation 4. The predicted frozen section thickness S_f of specimens at different water contents decreases steadily as wave velocity increases, but the slope of the relationship is low. This indicates that the sensitivity of S_f to v_f is low at different water contents.

For the purpose of prediction, v_f can be approximated to wave velocity at −10°C because the design average temperature in the field is usually −10°C. The predicted results of frozen section thickness thus given are presented in Table 2. Generally, the accuracy of predictions ranges from 86.84 to 99.33%, which indicates the values predicted by Equation 4 were subject to only small errors.

4.2.2 | Frozen wall thickness in the field

Frozen section thickness measured in laboratory testing can be treated as a simplified model of frozen wall thickness in the field. Therefore, the latter can be calculated using Equation 4. Based on our experimental results, S is 1,470 mm, v_u of fine sand approximates that of undisturbed soil (1.741 km/s), and τ_p is a measured value of different freezing periods (24, 26, and 42 days). v_f approximates wave velocity at −10°C measured in the field (4.884 km/s). The predicted values of frozen wall thickness in the field are given in Table 3. Measured values of frozen wall thickness in Table 3 were obtained by a temperature sensor (diameter 4 mm and length 30 mm) in steel pipes J_1 and J_2, where the thickness is determined for sand whose temperature is <0°C (Figure 16).

As shown in Table 3, the accuracy of predictions ranges from 90.32 to 98.03%, which indicates that the errors were small. Thus, Equation 4 also can be used to estimate frozen wall thickness in fine sand for field purposes.

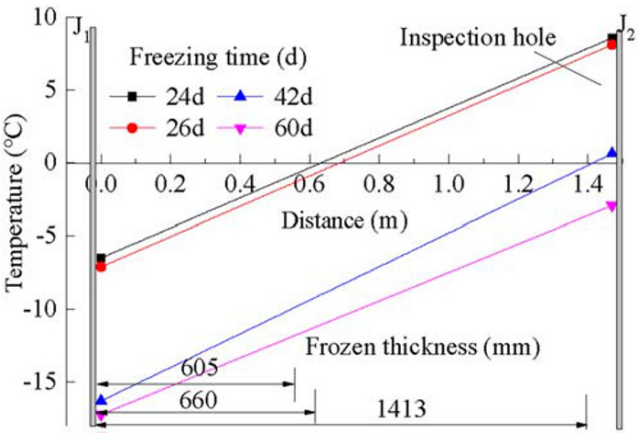

FIGURE 16 Measured values of frozen wall thickness determined from monitoring of ground temperature at different times of freezing at inspection holes J_1 and J_2 [Colour figure can be viewed at wileyonlinelibrary.com]

4.3 | Implications for frozen ground engineering

As illustrated above, the receiving ultrasonic wave velocity can reflect the freezing state and be used to calculate the cryofront position. Frequency components can reveal the frequency of different evolving freezing regions and freezing state during progressive freezing. As a result, this technique can be used in artificial ground frozen engineering, where it is difficult to accurately determine the freezing state and frozen wall thickness along the direction of frozen wall development because of a limited number and fixed position of thermometer holes. Ultrasonic testing can be used as a convenient and quick method of evaluating frozen wall development. First, the average temperature of frozen soil can be measured by the wave velocity and dominant frequency in any two freezing holes.[23] Frequency components and wave velocity in different freezing periods can then be compared to identify the freezing state between two holes (e.g., freezing hole, temperature monitoring hole and hydrological hole). Finally, frozen wall thickness during the active freezing period can be calculated between any two holes.

5 | CONCLUSIONS

The following conclusions are drawn from this study:

1. Analysis of ultrasonic time-domain characteristics showed that wave velocity continually increased as the cryofront ascended the specimens of fine sand, and wave amplitude decreased initially and increased subsequently with rising cryofront position. Wave velocity, unlike wave amplitude, can reveal the cryofront position during progressive freezing.

2. Analysis of ultrasonic frequency-domain characteristics demonstrated that the frequency components during later stages of progressive freezing can reveal the natural frequency of different freezing regions.

3. Comparison of laboratory and field observations indicated that single and multiple peaks in the frequency spectrum and KFS during different stages of freezing can identify the freezing state.

4. An equation is proposed to calculate the thickness of the frozen section. Laboratory and field observations revealed that the accuracy of predicted values of the frozen section thickness ranges from 86.8 to 99.33%, and the equation can be used to predict frozen wall thickness in the field.

ACKNOWLEDGEMENTS

The research was financially supported by the National Natural Science Foundation of China (Grant Nos. 51804157; 5177040737; 11702094), the National Key Research and Development Plan of China (Grant No. 2016YFC0600904), the China Scholarship Council (Grant No. 201909110045), the Science and Technology Innovation Fund of TianDi Science and Technology Co., Ltd (Grant No. 2018-TD-QN008; 2018-TD-ZD004; 2019-TD-QN009), and the North China Institute of Science and Technology Applied Mathematics Innovation Team (Grant No. 3142018059), which are all gratefully acknowledged.

ORCID

Ji-wei Zhang https://orcid.org/0000-0003-3273-5581

Julian Murton https://orcid.org/0000-0002-9469-5856

REFERENCES

1. Armaghani DJ, Amin MFM, Yagiz S, Faradonbeh RS, Abdullah RA. Prediction of the uniaxial compressive strength of sandstone using various modeling techniques. *Int J Rock Mech Min Sci*. 2016;85:174-186. https://doi.org/10.1016/j.ijrmms.2016.03.018
2. Vitel M, Rouabhi A, Tijani M, Guérin F. Thermo-hydraulic modeling of artificial ground freezing: application to an underground mine in fractured sandstone. *Comput Geotech*. 2016;75:80-92. https://doi.org/10.1016/j.compgeo.2016.01.024
3. Russo G, Corbo A, Cavuoto F, Autuori S. Artificial ground freezing to excavate a tunnel in sandy soil. Measurements and back analysis. *Tunn Undergr Sp Tech*. 2015;50:226-238. https://doi.org/10.1016/j.tust.2015.07.008
4. Pimentel E, Papakonstantinou S, Anagnostou G. Numerical interpretation of temperature distributions from three ground freezing applications in urban tunnelling. *Tunn Undergr Sp Tech*. 2012;28:57-69. https://doi.org/10.1016/j.tust.2011.09.005
5. Alzoubi MA, Madiseh A, Hassani FP, Sasmito AP. Heat transfer analysis in artificial ground freezing under high seepage: validation and heatlines visualization. *Int J Therm Sci*. 2019;139:232-245. https://doi.org/10.1016/j.ijthermalsci.2019.02.005
6. Huang S, Guo Y, Liu Y, Ke L, Liu G. Study on the influence of water flow on temperature around freeze pipes and its distribution optimization during artificial ground freezing. *Appl Therm Eng*. 2018;135:435-445. https://doi.org/10.1016/j.applthermaleng.2018.02
7. Dolgov OA. *Calculation procedure of deep rock freezing in shaft sinking. Zamorazhivanie gornykh porodo pri prokhodke stvolov shakht (Rock Freezing in Shafting)*. Moscow, Russia: AN SSSR; 1961:9-64.
8. Sanger FJ, Sayles FH. Thermal and rheological computations for artificially frozen ground construction. *Eng Geol*. 1979;13(1):311-337. https://doi.org/10.1016/0013-7952(79)90040-1
9. Yang P, Ke JM, Wang JG, Chow YK, Zhu FB. Numerical simulation of frost heave with coupled water freezing, temperature and stress fields in tunnel excavation. *Comput Geotech*. 2006;33(6):330-340. https://doi.org/10.1016/j.compgeo.2006.07.006
10. Hu J, Hui Z, Xiao BW. Numerical analysis of temperature field of cup-shaped frozen soil wall reinforcement at shield shaft. In: applied mechanics and materials. *Appl Mech Mater*. 2013;341:1467-1471. https://doi.org/10.4028/www.scientific.net/amm.341-342.1467
11. Song L, Yang W, Huang J, Li H, Zhang X. GPR utilization in artificial freezing engineering. *J Geophys Eng*. 2013;10(3):034004;1-10. https://doi.org/10.1088/1742-2132/10/3/034004
12. Kurfurst PJ. Ultrasonic wave measurements on frozen soils at permafrost temperatures. *Can J Earth Sci*. 1976;13(11):1571-1576. https://doi.org/10.1139/e76-163
13. Nakano Y, Martin RJ III, Smith M. Ultrasonic velocities of the dilatational and shear waves in frozen soils. *Water Resour Res*. 1972;8(4):1024-1030. https://doi.org/10.1029/wr008i004p01024
14. Nakano Y, Arnold R. Acoustic properties of frozen Ottawa sand. *Water Resour Res*. 1973;9(1):178-184. https://doi.org/10.1029/wr009i001p00178
15. Thimus JF, Aguirre-Puente J, Cohen-Tenoudji F. Determination of unfrozen water content of an overconsolidated clay down to −160 C by sonic approaches—comparison with classical methods. *Ground Freezing*. 1991;91:83-88.
16. Wang DY, Zhu YL, Ma W, Niu YH. Application of ultrasonic technology for physical–mechanical properties of frozen soils. *Cold Reg Sci Technol*. 2006;44(1):12-19. https://doi.org/10.1016/j.coldregions.2005.06.003

17. Christ M, Park J-B. Ultrasonic technique as tool for determining physical and mechanical properties of frozen soils. *Cold Reg Sci Technol*. 2009;3(58):136-142. https://doi.org/10.1016/j.coldregions.2009.05.008
18. Li D, Ming F, Huang X, Zhang Y. Application of ultrasonic technology for measuring physical and mechanical properties of frozen silty clay. *Cold Regions Engineering*. 2015;1-12. https://doi.org/10.1061/9780784479315.001
19. Li D, Huang X, Ming F, Yu Z. The impact of unfrozen water content on ultrasonic wave velocity in frozen soils. *Procedia Eng*. 2016;143:1210-1217. https://doi.org/10.1016/j.proeng.2016.06.114
20. Huang X, Li D, Ming F, Bing H. Experimental study on acoustic characteristics and Physico-mechanical properties of frozen silty clay. *Chin J Rock Mech Rock Eng*. 2015;34:1489-1496. (in Chinese)
21. Wang P, Xu J, Fang X, Wang P, Zheng G, Wen M. Ultrasonic time-frequency method to evaluate the deterioration properties of rock suffered from freeze-thaw weathering. *Cold Reg Sci Technol*. 2017;143:13-22. https://doi.org/10.1016/j.coldregions.2017.07.002
22. Wang Y, Li X, Zheng B. Experimental study on mechanical properties of clay soil under compression by ultrasonic test. *Eur J Environ Civ Eng*. 2018;22(6):666-685. https://doi.org/10.1080/19648189.2016.1217791
23. Zhang JW, Liu ZQ, Shan RL, Zhou HQ. Review and prospect of abnormal condition of shaft frozen wall monitoring technique in complex formation condition. *Coal Sci Technol*. 2019;47.1:103-109. (in Chinese)
24. Sheng S, Wu L, Xu B, et al. *GB50123–1999, Standard for geotechnical test methods*. Nanjing, China: China Planning Press; 1999 (in Chinese).
25. Li C, Cui H, Liu X, et al. *MT/T593.8–2011, Artificial frozen soil test sampling and sample preparation method*. Beijing, China: Coal Industry Press; 2011 (in Chinese).
26. Wei Z, Ma J, Jin Y, et al. *JB/T 8428–2015, General specification for ultrasonic test specimen*. Shandong, China: China Machine Press; 2015 (in Chinese).
27. Yang P, Li Q, Yu CH. An experimental study on the acoustic wave parameters of artificial frozen soil. *J Glaciol Geocryol*. 1997;2:55-59. (in Chinese)
28. Ottosen N, Ristinmmaa M, Davis A. Theoretical interpretation of impulse response tests of embedded concrete structures. *J Eng Mech*. 2004;130(9):1062-1071. https://doi.org/10.1061/(asce)0733-9399(2004)130:9(1062)
29. Kawaguchi T, Mitachi T, Shibuya S. Evaluation of shear wave travel time in laboratory bender element test. In *Proceedings of the 15th* International Conference on Soil Mechanics and Geotechnical Engineering (ICSMGE), 2001; 1: 155–158.
30. Inci G. Nondestructive evaluation of compacted clayey soils. Internal Report, Department of Civil and Environmental Engineering, Wayne State University, Detroit, Michigan; 2000.
31. Amin G, Hedayat A. Ultrasonic investigation of granular materials subjected to compression and crushing. *Ultrasonics*. 2018;87:112-125.
32. Cote GL, Fox MD. Comparison of zero crossing counter to FFT spectrum of ultrasound Doppler. *IEEE Trans Biomed Eng*. 1988;35(6):498-502. https://doi.org/10.1109/10.2124
33. Alleyne DN, Cawley P. Optimization of lamb wave inspection techniques. *NDT & E Int*. 1992;25(1):11-22. https://doi.org/10.1016/0963-8695(92)90003-y
34. Ito Y, Uomoto T. Nondestructive testing method of concrete using impact acoustics. *NDT & E Int*. 1997;30(4):217-222. https://doi.org/10.1016/s0963-8695(96)00059-x
35. Lee HK, Lee KM, Kim YH, Yim H, Bae DB. Ultrasonic in-situ monitoring of setting process of high-performance concrete. *Cem Concr Res*. 2004;34(4):631-640. https://doi.org/10.1016/j.cemconres.2003.10.012
36. Hola J, Lukasz S, Krzysztof S. Nondestructive identification of delaminations in concrete floor toppings with acoustic methods. *Autom Construct*. 2011;20(7):799-807. https://doi.org/10.1016/j.autcon.2011.02.002
37. Pyrak-Nolte LJ. The seismic response of fractures and the interrelations among fracture properties. In: *International Journal of Rock Mechanics and Mining Sciences & Geomechanics Abstracts*. Oxford, UK: Pergamon; 1996:787-802. https://doi.org/10.1016/s0148-9062(96)00022-8
38. Rinkevich AB, Perov DV. A wavelet analysis of acoustic fields and signals in ultrasonic nondestructive testing. *Russ J Nondestr Test*. 2005;41(2):93-101. https://doi.org/10.1007/s11181-005-0134-5
39. Ni SH, Lo KF, Lehmann L, Huang YH. Time–frequency analyses of pile-integrity testing using wavelet transform. *Comput Geotech*. 2008;35(4):600-607. https://doi.org/10.1016/j.compgeo.2007.09.003
40. Kong Q, Wang R, Song G, Yang ZJ, Still B. Monitoring the soil freeze-thaw process using piezoceramic-based smart aggregate. *J Cold Regions Eng*. 2014;28(2):06014001;1-16. https://doi.org/10.1061/(asce)cr.1943-5495.0000066
41. Spiegel MR, Stephens LJ. *Schaum's Outline of Theory and Problems of Statistics*. New York, NY: McGraw Hill; 1961.

How to cite this article: Zhang J, Murton J, Liu S, Sui L, Zhang S. Detection of the freezing state and frozen section thickness of fine sand by ultrasonic testing. *Permafrost and Periglac Process*. 2020;1–16. https://doi.org/10.1002/ppp.2075